Cell Type Specific Aging Transcriptional Signatures of Human Retina Through Integrated Machine Learning and Single-Cell Transcriptomics

Luning Yang[1], Sen Lin[1], Yiwen Tao[1], Qi Pan[1], Tengda Cai[1], Yunyan Ye[2], Jianhui Liu[3], Yang Zhou[4], Yongqing Shao[5], Quanyong Yi[5], Zen Huat Lu[6], Lie Chen[6], Gareth McKay[7], Richard Rankin[8], Fan Li[9*], Weihua Meng[1,10,11*]

1 Nottingham Ningbo China Beacons of Excellence Research and Innovation Institute, University of Nottingham Ningbo China, Ningbo, China, 315100

2 Department of Ophthalmology, Lihuili Hospital affiliated with Ningbo University, Ningbo, China, 315040

3 Department of Cardiology, Lihuili Hospital affiliated with Ningbo University, Ningbo, China, 315040

4 Ningbo Institute of Innovation for Combined Medicine and Engineering, The Affiliated Li Huili Hospital, Ningbo University, Ningbo, China, 315201

5 Department of Ophthalmology, The Affiliated Ningbo Eye Hospital of Wenzhou Medical University, Ningbo, China, 315040

6 PAPRSB Institute of Health Sciences, Universiti Brunei Darussalam, Bandar Seri, Begawan, Brunei Darussalam, BE1410

7 Centre for Public Health, Institute of Clinical Science, Queen's University Belfast, Block B, Royal Hospital, Grosvenor Road, Belfast, UK, BT12 6BA

8 Centre for English Language Education, University of Nottingham Ningbo China, Ningbo, China, 31510

9 Eye Center, Zhongshan City People's Hospital, Zhongshan, Guangdong, China, 528403

24 10 Division of Population Health and Genomics, School of Medicine, University of Dundee,
25 Dundee, UK, DD2 4BF

26 11 Center for Public Health, Faculty of Medicine, Health and Life Sciences, School of
27 Medicine, Dentistry and Biomedical Sciences, Queen's University Belfast, Belfast, UK, BT12
28 6BA

29 Luning Yang and Sen Lin contributed equally to this paper.

30

31 Corresponding Author:

32 Dr Weihua Meng

33 Address: Nottingham Ningbo China Beacons of Excellence Research and Innovation Institute,
34 University of Nottingham Ningbo China, Ningbo, China, 315100. Tel: +86 574 88188632.
35 Email: weihua.meng@nottingham.edu.cn. ORCID: 0000-0001-5388-8494

36 Dr Fan Li

37 Address: Eye Center, Zhongshan City People's Hospital, No.2 East-sun-wen Road,
38 Zhongshan, Guangdong, China, 528403. Tel: +86 13430260377. Email: lifan82@126.com.
39 ORCID: 0000-0001-7318-3002

40

Abstract

Single-cell RNA sequencing (scRNA-seq) has significantly advanced our understanding of retinal aging, yet the specific molecular characteristics within cell populations remain incompletely defined. We profiled 223,612 single cells from 18 unfrozen human retinas obtained from 13 Chinese donors aged 34–92 years, providing an ethnically specific atlas across the adult lifespan. A sparsity-driven machine-learning (ML) pipeline (L1-regularized logistic regression, recursive feature elimination with cross-validation) identified age-discriminatory genes within each major retinal cell type, complemented by gene set scoring for cellular senescence and metabolic pathways. Using integrated differential expression and ML feature selection, we identified eleven major retinal cell populations and observed aging-associated shifts. ML classifiers achieved high accuracy (80–96%), particularly for microglia (96%), revealing mitochondria-centric aging signatures in rods and bipolar cells, proteostasis and retinoid metabolism in cones, and structural-RNA maintenance signatures in horizontal cells. This study delivers the first ML-derived, cell-type-specific aging gene signatures for the human retina in a Chinese cohort, offering a reference for population-tailored biomarker discovery.

Keywords: aging, retina, single-cell RNA sequencing, machine learning, transcriptional regulation

Introduction

Aging is a fundamental biological process characterized by progressive functional and structural decline across multiple organ systems, including the retina [1,2]. Age-related retinal deterioration disrupts visual function, impairing acuity and quality of life, and increases vulnerability to retinal diseases such as age-related macular degeneration (AMD) and diabetic retinopathy (DR) [3-5]. Understanding the mechanisms underlying retinal aging is essential for developing strategies to preserve vision in aging populations [6,7].

Advances in high-resolution transcriptomic technologies, particularly single-cell RNA sequencing (scRNA-seq), have significantly enhanced our understanding of retinal aging by enabling detailed profiling of cellular heterogeneity and molecular dynamics [8-10]. Recent scRNA-seq studies have revealed progressive transcriptional changes across retinal cell types during aging. In 2020, human and macaque analyses identified a foveal-to-peripheral aging gradient and *MYO9A*-negative rod vulnerability [9]. By 2025, mouse studies uncovered transcriptionally distinct rod subpopulations with differential aging responses and bipolar cell (BC) shifts linked to scotopic vision decline [8]. However, critical limitations persist. Large-scale human retina transcriptomic datasets predominantly feature samples from white populations [11,12], limiting ethnic-specific differences often underexplored. While initiatives like the Human Cell Atlas have mapped retinal development across 122 donors, only 5 Asian donors were included in its most comprehensive dataset to date [13]. Furthermore, smaller studies often lack adequate representation of younger age groups, potentially missing early molecular changes that preceded structural or functional deficits. Ethnic variations in retinal characteristics—such as macular pigment density and retinal layer thickness—necessitate diverse cohorts for generalizable insights [14-16].

78 To address these limitations, we characterize the age-dependent transcriptional landscape of the human
79 retina using scRNA-seq in a cohort of 18 Chinese donors aged 34-92 years. Unique strengths of our
80 dataset are the inclusion of early-age samples providing insights into initial stages of retinal aging,
81 ethnic-specific characterization addressing representation gaps in Chinese populations. This study aims
82 to define age-dependent changes in retinal cellular composition, identify transcriptional signatures of
83 retinal aging, and elucidate underlying regulatory networks. This study integrates conventional
84 differential expression analysis with L1-regularized logistic regression and recursive feature
85 elimination to identify cell-type-specific aging signatures that transcend traditional statistical
86 thresholds.

87

88 ## Methods

89 **Retinal Sample Collection**

90 Human retinas were collected from living and cadaveric donors under protocols approved by the ethics
91 committees of the University of Nottingham Ningbo China, the Ningbo Lihuili Hospital, and the
92 Ningbo Eye Hospital. Living donor samples were processed within 10 min post-enucleation, and
93 cadaveric samples within 6 h postmortem. Retinal specimens were collected without regional
94 dissection to ensure comprehensive coverage.

95 **Donor Demographics**

96 We analyzed 18 retinal samples from 13 donors, stratified into young (34-55 years, n=9) and old (68-92
97 years, n=9) groups. Eight samples were from individuals with DR, evenly distributed across age groups.
98 Table 1 provides donor details, including disease status and reasons for enucleation or death.

99 **Retinal Tissue Dissociation**

100 Retinal tissues were dissociated using the LK003150-1bx Dissociation Kit (Worthington Biochemical
101 Corporation). Tissues were minced into fragments and incubated at 37 ℃ for 30 min with gentle
102 agitation. Dissociation was performed using a gentleMACS C tube, followed by filtration through a 70
103 μm cell strainer. Red blood cells were lysed using Red Blood Cell Lysis Solution (Miltenyi Biotec),
104 and viable cells were counted using AO/PI fluorescent dye with CountStar analysis. Cell suspensions
105 with viability >85% were resuspended in 0.04% BSA/PBS at 700–1200 cells·μL^{-1}.

106 **scRNA-seq library preparation**

107 Single-cell suspensions were processed using the Chromium Single Cell 3' Library and Gel Bead Kit
108 v3.1 (10x Genomics). Approximately 10,000 cells per sample were loaded onto the Chromium
109 Controller to generate gel beads in emulsion (GEMs). Reverse transcription within GEMs produced
110 barcoded cDNA, followed by amplification, fragmentation, and adapter ligation. Libraries were
111 sequenced (Illumina NovaSeq, 150 bp paired-end), and quality was assessed with FastQC.

112 **scRNA-seq Data Processing and Analysis**

113 Raw sequencing data were processed using Cell Ranger v8.0.1 (10x Genomics) for demultiplexing,
114 alignment to the human reference genome (GRCh38-2020-A), barcode filtering, and UMI
115 quantification. Quality control was performed using a dynamic thresholding approach based on median
116 absolute deviation statistics to adaptively filter cells. Retained cells expressed ≥200 genes, had UMI
117 counts >500, and <15% mitochondrial transcripts. Doublets were identified and removed using
118 DoubletFinder v2.0.4 [17]. Integrated analysis of scRNA-seq datasets was performed using Scanpy
119 v1.10.2 with batch-effect correction via scVI-tools v0.17.1 [18,19]. Highly variable genes were selected
120 for dimensionality reduction using latent space embedding. A k-nearest neighbor graph was constructed
121 for Leiden clustering at multiple resolutions to identify major retinal cell types. Marker gene expression

122 was used for cell type annotation across clusters based on corresponding marker genes.

123 **Rod Contamination Filtering**

124 To minimize technical artifacts from rod contamination in non-rod populations, we implemented a
125 systematic filtering approach. Rod-specific expression scores were calculated for each cell using
126 canonical photoreceptor markers (*RHO*, *PDE6B*, *GNAT1*) via Scanpy's score_genes function. Optimal
127 thresholds were determined by identifying local minima in kernel density estimation plots of the score
128 distribution. For non-rod population analyses, cells exceeding the algorithm-determined threshold were
129 excluded, while rod-specific analyses retained only cells above threshold.

130 **Age-dependent Differential Expression Analysis**

131 Age-dependent transcriptional changes across retinal cell populations were examined using
132 complementary single-cell differential expression (SC-DE) and pseudobulk differential expression
133 (PB-DE) approaches. For SC-DE, cells were grouped by cell type and age category (young vs. old),
134 with differentially expressed genes (DEGs) identified using likelihood-ratio tests in Seurat v5.1.0 (FDR
135 < 0.05, $|\log_2 FC| > 0.25$) [20]. For PB-DE, expression counts were aggregated by cluster-sample
136 combinations and analyzed with DESeq2 v1.42.1 (design: ~ batch + age_group) [21]. Following
137 normalization and dispersion estimation, significance was determined using Wald tests with apeglm
138 shrinkage (adjusted $P < 0.05$, with $|\log_2 FC|$ thresholds ≥ 0). Results identified three categories of
139 age-associated genes: exclusively SC-DE, exclusively PB-DE, and high-confidence DEGs from both
140 methods.

141 **Pathway Enrichment Analysis**

142 Pathway enrichment was conducted using the irGSEA v3.3.2 [22], integrating scoring methods, including
143 AUCell, UCell, singscore, ssgsea, JASMINE, and viper. Hallmark gene sets from MSigDB [23] were

144 used as reference pathways. Enrichment scores were calculated for each cell type and age group.
145 Results were aggregated using robust rank aggregation to obtain consensus enrichment scores.
146 Significantly enriched pathways were defined as those with an adjusted $P < 0.05$.

147 **Multi‐Stage Machine Learning (ML) Based Key Genes Selection**

148 A multi‐stage, rigorously controlled ML framework to identify age‐stage marker genes in each
149 retinal cell type was implemented. Firstly, for each old‐versus‐young comparison, we curated
150 the top 200 genes by absolute $\log_2$ ‐fold change from DEGs and extracted their expression
151 profiles for z‐score normalization. The normalized matrix was then stratified into 70 % training
152 and 30 % testing subsets, with all features mean‐centered and variance‐scaled to conform to
153 linear‐model prerequisites. Then, L1‐regularized logistic regression was applied, optimizing
154 the penalty hyperparameter C (0.01–10) via 5‐fold cross-validation grid search to enforce model
155 sparsity. Building upon this tuned model, recursive feature elimination with internal
156 cross‐validation (RFECV) was employed, systematically removing the least contributory genes
157 until maximal cross‐validated performance was attained. To validate the robustness of these key
158 genes, we repeated RFECV across 20 bootstrap replicates, retaining only those genes selected in
159 over 50 % of runs. Model performance on the test set was evaluated by precision, recall, and
160 F1‐scores, complemented by ROC curves and AUC metrics for each class. By integrating L1
161 penalization, RFECV, and stability selection, this ML based framework yielded an important and
162 stable gene signature for age‐stage classification.

163 **Transcription Factor Regulatory Network Inference**

164 Transcription factor (TF) regulatory networks were inferred using pySCENIC (v1.2.2) [24] to identify key
165 transcriptional regulators across retinal cell populations during aging. For computational efficiency,

166 5,000 cells were randomly sampled from each dataset and processed into cell type-specific subsets for
167 interneurons and glial cells. Co-expression modules were identified with GRNBoost2 with official list
168 of human TFs (https://resources.aertslab.org/cistarget/tf_lists/), followed by cis-regulatory motif
169 analysis using RcisTarget with hg38 motif rankings (10kb up/downstream of transcription start sites).
170 Regulon activity scores were computed using AUCell and binarized to determine active regulons in
171 individual cells. Regulon specificity scores were calculated to identify condition-specific
172 transcriptional regulators.

173 **Gene Set Scoring Analysis in Aging Retinal Cell Types**

174 Gene set scoring was performed to evaluate pathway activity across retinal cell types during aging
175 using the UCell package (v2.6.2) [25]. Predefined gene sets, including cellular senescence (SenMayo) [26]
176 and genes related to polyamine metabolism (see Supplementary Table S1). Statistical comparisons of
177 pathway scores between young and old age groups were conducted using Wilcoxon rank-sum tests,
178 with significance defined at $P<0.05$.

179

180 Results

181 **Age-Related Shifts in Retinal Cellular Composition**

182 We performed scRNA-seq analysis of 18 retinal samples from young and older adults. Unsupervised
183 clustering identified 11 major retinal cell populations (Figs. 1a, 1b) with the summary table in
184 Supplementary Table S2. For aging analysis, we focused on glial cells, photoreceptors, and
185 interneurons, excluding T cells (variable proportions) and retinal pigment epithelium (RPEs)/ retinal
186 ganglion cells (low cell counts). Quantitative assessment revealed distinct age-related compositional
187 changes. The rod-to-cone ratio showed a decreasing trend with advancing age (Fig. 1c). Among

188 interneurons, the BC / (amacrine cell [AC] + BC + horizontal cell [HC]) ratio displayed a downward
189 trend, suggesting a relative BC decrease with age (Fig. 1d). Within glial populations, astrocytes
190 exhibited the most pronounced age-related changes, with their relative proportion showing a clear
191 upward trend with advancing age, while Müller glial cells (MGCs) consistently represented the
192 majority of glial cells across age groups (Figs. 1e-g).

193 Further analysis of identified BC subtypes (Figs. 2a, 2b) revealed distinct age-related patterns (Fig. 2c)
194 with summary shown in Supplementary Table S3. Rod BCs (RB) consistently represented the largest
195 proportion among BC subtypes (median 26%), with an outlier at age 50 (68.85%). Among diffuse BCs
196 (DB), DB2 and DB3b were the most abundant, with DB2 showing higher proportions in middle-aged
197 samples (~12.88% at age 69) and lower values in older samples (~6.57% at age 92). DB4a exhibited a
198 gradual decline with age (14.47% at age 34 to ~8.97% at age 69), while DB4b remained consistently
199 below 2%. Midget BCs showed divergent patterns: Invaginating midget BCs (proportions remained
200 relatively stable across ages (~10-16%), while flat midget BCs showed greater variability, peaking at
201 15.79% at age 55 and declining to ~5% in older samples.

202

203 **Comprehensive Profiling of Aging Retina Uncovers Cell- Type- Specific DEGs and Shared**
204 **Hallmarks**

205 Having characterized the age-related shifts in retinal cellular composition, we next aimed to delineate
206 the underlying molecular alterations by performing a comprehensive transcriptional analysis across
207 major retinal cell types. Transcriptional profiling revealed cell type-specific differential gene
208 expression patterns across retinal cells with aging (Supplementary Table S4-S6). BCs exhibited the

209 most substantial transcriptional changes among interneurons with 1,171 DEGs (563 upregulated, 608
210 downregulated), compared to ACs (26 DEGs) and HCs (124 DEGs) (Fig. 2d). Among these, 96.7% of
211 BC DEGs were cell type-specific, compared to 53.8% in ACs and 71.8% in HCs, with 278
212 high-confidence genes detected by both analysis methods. Pathway analysis in interneurons identified
213 shared enrichment in hypoxia-related pathways, suggesting metabolic reprogramming as a fundamental
214 mechanism in retinal neuronal aging (Fig. 2e). BCs demonstrated pronounced inflammatory activation
215 (*CCL2*, *HLA-DRA*), gliosis (*GFAP*), and metabolic shifts toward glycolysis (*PFKFB4*, *PDK1*), along
216 with extensive mitochondrial gene downregulation. ACs showed upregulation of angiogenic signaling
217 (*VEGFA*) and mitochondrial quality control genes (*BNIP3*), while HCs exhibited unique enrichment in
218 TGF-beta signaling and stress response genes (*EGR1*, *TMSB10*). Despite cell type-specific responses,
219 conserved aging hallmarks emerged across all interneurons: mitochondrial dysfunction, immune
220 activation, and synaptic weakening.

221 Among glial cells, MGCs exhibited the most pronounced alterations (2,117 DEGs), followed by
222 microglia (276 DEGs) and astrocytes (74 DEGs) (Fig. 2f). Cell type specificity was highest in MGCs
223 (94.2%), compared to microglia (68.5%) and astrocytes (43.2%). Core genes upregulated across all
224 glial types included *FTH1* (iron sequestration), *LDHA* (glycolysis), and *SLC3A2* (amino acid transport),
225 while *MT-ND6* (mitochondrial function) was consistently downregulated. Pathway analysis confirmed
226 shared enrichment in Hypoxia, TNFA signaling via NF-kB, mTORC1 signaling, and EMT pathways
227 (Fig. 2g). Each glial subtype demonstrated distinctive transcriptional signatures: MGCs uniquely
228 displayed extensive inflammatory signaling (*CXCL1/2*) and matrix remodeling (*SERPINE1, LOX*);
229 astrocytes showed induction of stress-response factors (*DNAJB1, DDIT3*) with concurrent
230 downregulation of neuronal-supportive genes (*GRIA1, AQP4*). Comparative analysis with retinal

231 interneurons revealed shared aging mechanisms but distinct effector pathways: glial cells prominently
232 involved antigen-presentation, whereas interneurons primarily expressed chemokines.

233 Photoreceptors exhibited subtype-specific aging responses, with rods showing substantially greater
234 transcriptional changes (273 DEGs) than cones (67 DEGs) (Fig. 2h). Cell type-specificity analysis
235 revealed that 91.9% of rod DEGs were unique to rods versus 67.2% for cones. Both photoreceptor
236 types shared upregulation of stress response genes (*CRYAB, MT2A*) and chaperones (*BAG3*), while
237 commonly downregulating mitochondrial genes (*MT-ND6*) and cytoskeletal components (*KIF2A*).
238 Integrated pathway analysis confirmed enrichment of oxidative stress response and mitochondrial
239 dysfunction pathways in both cell types (Fig. 2i). Rods uniquely exhibited downregulation of
240 TNFA-signaling-via-NFKB pathways alongside significant upregulation of WNT-β-catenin signaling,
241 supported by increased expression of *WNT5B*, *WNT11* and *FZD3*. Rod-specific DEGs included
242 upregulated stress response genes (*S100A6*, *NLN*) and downregulated phototransduction-related genes
243 (*ELOVL4*, *CRB1*). Cones selectively downregulated fatty acid metabolism and protein secretion
244 pathways, with substantial decreases in membrane transport components. Compared to glial cells,
245 photoreceptors exhibited similar response patterns but with lower magnitude of transcriptional changes,
246 underscoring their specialized functional vulnerability during aging.

247

248 **Machine Learning Identifies Robust Transcriptional Features of Retinal Aging**

249 In the previous section, we performed DE and enrichment analysis to characterize aging-related
250 changes within major retinal cell types. To further identify the robust transcriptional discriminators of
251 cellular age, we applied a ML framework using a L1‑regularized logistic regression with

252 cross-validation. This approach ranked genes based on their importance in classification, providing a
253 prioritized list of robust age-defining features (Supplementary Table S7). Compared to traditional
254 feature analysis approaches, the ML model excelled at identifying subtle yet highly consistent changes
255 indicative of aging, including features with modest fold changes that might be overlooked in standard
256 statistical tests, particularly in regulatory elements and less abundant transcripts that nevertheless serve
257 as powerful age discriminators. Our ML models achieved high classification accuracy across all cell
258 types, ranging from 80% in astrocytes to 96% in microglia, with an average accuracy of 89%,
259 demonstrating strong classification power of the identified features (Table 2). The number of
260 ML-identified discriminatory features varied considerably between cell types, with patterns that
261 partially mirrored our DEG analysis but revealed important distinctions. Astrocytes showed the fewest
262 ML features (15), consistent with their limited DEGs (74), while MGCs had the most (199), aligning
263 with their extensive DEG count (2,117). Bipolar cells (180), rods (191), and cones (196) all exhibited
264 substantial ML features, indicating strong age-related transcriptional signatures (Fig. 3a). Notably,
265 cones presented a striking divergence between metrics-few DEGs (67) but abundant ML features (196),
266 suggesting that subtle, consistent transcriptional shifts that don't meet statistical thresholds for
267 differential expression can nonetheless serve as powerful age discriminators. This pattern was also
268 observed in ACs (105 ML features versus 26 DEGs).

269 The ML analysis consistently pinpointed genes central to cell-type-specific functions and critical
270 homeostatic pathways as top age classifiers. Firstly, analysis of transcriptional features recurring in
271 three or more retinal cell types, complement and reinforce the shared patterns of aging that discriminate
272 between young and old groups (Supplementary Table S8). Mitochondrial dysfunction emerges as a
273 dominant theme, with *MT-ND6* showing the highest frequency, suggesting Complex I impairment as

274 the most conserved aging signature. Proteostasis decline is evident through frequent chaperones such
275 as *CRYAB* and *HSPA1A*, and the ubiquitin system via *UBC*, indicating pan-retinal stress responses to
276 protein misfolding. Oxidative stress responses are widespread, marked by *GPX3* and metallothioneins
277 like *MT2A*, while low-grade inflammation is supported by immune genes including *HLA-A*
278 and *S100A10*. Structural integrity is also affected, with cytoskeletal changes via *TUBA1B*, synaptic
279 reorganization via *MAGI2*, and extracellular matrix remodeling via *P4HA1*. Beyond these established
280 hallmarks, novel players include transcriptional regulators *BHLHE40*, linked to hypoxia and circadian
281 disruption, and *ERO1A*, suggesting underappreciated stress response hubs. Additionally, non-coding
282 RNAs like *FTX* and *SNHG14* point to epigenetic regulation, while *NCL* (nucleolin) hints at nucleolar
283 stress, and *TF* (transferrin) indicates disrupted iron homeostasis, potentially exacerbating oxidative
284 damage. These findings reinforce classic aging themes while highlighting novel regulatory and
285 metabolic vulnerabilities in the aging retina.

286

287 **Cell-Type Specific ML Features Reveal Distinct Aging Vulnerabilities**

288 Our ML model of microglia demonstrated a high degree of accuracy (96%) in distinguishing between
289 young and old cells (Fig. 3b). This high performance, compared to other retinal cell types (which
290 averaged 89% accuracy), suggests that aging induces robust and consistent transcriptional changes in
291 these cells. Our recursive feature elimination with cross-validation approach identified the optimal
292 feature set for classification (Fig. 3c), ensuring model performance while minimizing overfitting.
293 Inspection of the top 20 importance ranks (Fig. 3d) reveals the dominant molecular programmes of
294 Metal–redox buffering, accompanied by Inflammation-linked matrix remodeling. A smaller third set

295 reflects metabolic and structural rewiring. Metallothioneins (*MT1E*, *MT1X*, *MT2A*) and ferritin subunits
296 (*FTH1*, *FTL*) occupied five positions among the top-ranked features, revealing a concerted response to
297 metal dysregulation as a defining hallmark of aged microglia. This metal-redox buffering signature has
298 been previously noted in photoreceptors but is now specifically pinpointed as a key distinguishing
299 feature in aged microglia cells, potentially indicating a tractable pathway for modulating glial
300 contributions to retinal senescence.

301 For astrocytes, classification accuracy was more modest at 80%, reflecting a focused 15-gene signature
302 related to acute-phase and protease regulation (Fig. 4a). Haptoglobin (*HP*) and serine-protease inhibitor
303 *SLPI* were among the top-ranked features, suggesting that aged retinal astrocytes activate systemic-like
304 acute-phase defenses, an underappreciated aspect of ocular aging.

305 The MGC classifier achieved 89% accuracy in five-fold cross-validation (Fig. 4b). Analysis of the
306 highest-weight features reveals three interconnected aging programs: mitochondrial distress (evidenced
307 by *MT-CO3*, *MT-ND6*, and *MT-ND3*), matrix remodeling (featuring *COL4A3*), and a distinctive
308 Ca^{2+} /Wnt-lipid signaling network. This third program combines Ca^{2+} sensor *CALM1*, Wnt pathway
309 inhibitor *WIF1*, and lipid/hypoxia response genes (*RORA*, *HILPDA*, and *ADM*). Our BC classifier
310 performed robustly at 91% accuracy, while AC reached 85% accuracy and HC achieved 93% accuracy
311 (Fig. 4c-e). In interneuron ACs and BCs, mitochondrial distress dominates-notably, eight of BC's top
312 ten features are mitochondrial transcripts (*MT-CO3*, *MT-CYB, MT-CO2, MT-ATP6, MT-ND2, MT-CO1*,
313 *MT-ND3, MT-ND5*), pointing to respiratory chain impairment as the principal discriminator of BC
314 aging. ACs similarly prioritize mitochondrial genes (*MT-ATP6, MT-ND6, MT-CO2*) but additionally
315 elevate the mitophagy trigger *BNIP3*. While MGCs display only modest mitochondrial signal, their
316 Ca^{2+} machinery integrates with tissue-modulatory networks. Each cell type shows distinct

317 proteostasis-lipid-immune signatures: ACs feature chaperone *HSP90AA1*, ER-reticulon *RTN3*, lipid
318 enzyme *HMGCS1* , and *MHC-I HLA-C*; BCs include circadian/hypoxia regulator *BHLHE40*; and
319 MGCs highlight matrix-gliosis gene *COL4A3* and vasopeptide *ADM*. HCs break the pattern
320 entirely-their top features are cytoskeletal and synaptic scaffolds (*SEPTIN4, TUBA1B, STMN4,*
321 *DCLK1*), alongside a unique RNA-chaperone module (*SNHG14, FTX , CRYAB, HSPE1, FUS*) and
322 signaling modulators (*PDE4B , GRIA4*). This analysis reveals that aging manifests as energy failure in
323 AC/BC, metabolic-paracrine rewiring in MGC, and structural-RNA maintenance in HC.

324 Rods (89% accuracy, AUC = 0.95) are dominated by a dual axis of mitochondrial respiratory-chain
325 failure-six MT-encoded OXPHOS transcripts (e.g., *MT-CO3, MT-ND3, MT-CO2, MT-CO1, MT-ND2,*
326 *MT-CYB*) together with a broad heat-shock/ubiquitin response (*HSPA1A, UBB, HSP90AB1, DNAJB1*),
327 indicating that ageing rods depend on sustained ATP supply and intensive protein-quality control (Fig.
328 4f). Cones deliver comparable performance (90% accuracy, AUC = 0.96) yet place no mitochondrial
329 genes within their top 20 features (Fig. 4g); instead, they emphasise chaperone-ribosome stress
330 (*HSPH1, DNAJB1, RPS26*) and outer-segment membrane/retinoid maintenance (*TTR, ROM1, BCO2,*
331 *THSD7B*). Thus, ageing photoreceptors converge on proteostasis yet diverge into mitochondria-centric
332 (rods) versus membrane-metabolite (cones) adaptations. Unlike inner neurons, they couple protein
333 surveillance directly to phototransduction architecture, highlighting distinct therapeutic entry points for
334 preserving scotopic versus photopic vision in the ageing retina. The results suggest that rods and cones
335 follow appreciably different ageing routes-rods showing a mitochondria-plus-ubiquitin stress axis,
336 while cones favour a proteostasis-retinoid/membrane programme-highlighting cell-type-specific
337 priorities that could inform future strategies for protecting scotopic and photopic vision.

338

339 **Regulatory Network Alterations with Aging Human Retina**

340 SCENIC analysis revealed both shared and cell type-specific TF regulatory patterns in aging retinal
341 interneurons (Fig. 3e; see Supplementary Table S9). Across all 3 interneuron types, stress-responsive
342 TFs *BHLHE40* and *MXI1* showed consistently increased regulon activity, indicating a conserved
343 hypoxia-driven metabolic stress response. Notably, *BHLHE40* was also identified as one of the top
344 aging features by BCs ML model, underscoring its importance in interneuron aging. *CHD1* regulon
345 activity was significantly elevated, suggesting chromatin remodeling accompanies cellular stress
346 responses. Conversely, neuronal identity TF *NEUROD1* exhibited reduced regulon activity, potentially
347 contributing to synaptic dysfunction, while ATF-family TFs showed diminished regulon activities,
348 suggesting a decrease in proteostatic. Each interneuron type displayed distinctive regulatory signatures.
349 ACs exhibited unique *PROX1* regulon activation (reduced in BCs) alongside elevated *NFIA* and *TCF4*
350 regulons. BCs showed pronounced inflammatory signatures through increased *NFKB1* regulon activity,
351 aligning with upregulated inflammatory genes (*CCL2*, *HLA-DRA*) from our differential expression
352 analysis. HCs displayed distinctive *IRF1* regulon activation and compromised identity maintenance
353 through substantial decreases in *ONECUT1* activity.

354 Gene set scoring analysis revealed significant decreases in polyamine metabolism pathway activity in
355 aged cells across all interneuron types, suggesting impaired cellular homeostasis (Fig. 3f). Conversely,
356 cellular senescence gene set (SenMayo) activity increased significantly in all 3 cell types (Fig. 3g).

357 SCENIC analysis revealed conserved activation of stress-responsive TFs across all glial cell types
358 during aging (Fig. 5a; see Supplementary Table S10). *XBP1*, *JUND*, *FOSL2*, *MAFF*, *BHLHE40*, and
359 *BHLHE41* showed increased regulon activity in astrocytes (obvious elevation), microglia (moderate
360 elevation), and MGC (variable elevation), highlighting conserved regulatory mechanisms related to

361 cellular stress, inflammation, and metabolic reprogramming. Each glial subtype exhibited distinctive
362 regulatory signatures. MGC uniquely showed significant *ZXDA*(-) regulon activity reduction,
363 suggesting altered chromatin remodeling. Microglia specifically displayed increased regulon activity of
364 hypoxia-responsive (*MITF*, *MXI1*) and metabolic TFs (*FOSL1*), alongside reduced regulon activity of
365 immune-related regulons (*RFXANK*). Astrocytes demonstrated substantial induction of stress-response
366 (*CEBPB*, *HOXA5*) and lipid metabolism (*SREBF1*) regulons. While both interneurons and glia showed
367 increased stress-responsive TF regulon activity with age, glial cells exhibited more pronounced
368 differential activity, particularly with strong *ZBTB21* regulon activation in aged MGCs and astrocytes,
369 and consistent *MAFF* elevation across all glial cells. In addition to these changes, TF analysis revealed
370 distinct regulatory profiles in rods and cones, detailed in Supplementary Table S11.
371 Gene set scoring analysis revealed differential metabolic resilience among glial subtypes. Polyamine
372 metabolism gene set activity decreased significantly only in aging MGC, while microglia and
373 astrocytes maintained stable activity (Fig. 5b). The SenMayo cellular senescence gene set showed
374 robust increased activity across all glial types, particularly in astrocytes and MGC, exceeding the
375 magnitude observed in interneurons and suggesting a more prominent role for glial senescence in
376 retinal aging (Fig. 5c).
377

378 **Discussion**

379 Although scRNA-seq transcriptomic studies have explored retinal aging at various biological levels,
380 compared to AMD, the physiological aging of human retina has received less attention, despite being
381 the foundation for late-onset retinal diseases. Current single-cell retinal aging studies have been
382 constrained by limited sample sizes, incomplete age representation across the adult lifespan, and

383 predominant focus on cohorts of Caucasian ancestry. Moreover, while ML models have been widely
384 adopted for feature selection and predictive analysis in various biological domains [27-30], their
385 application in human retinal aging transcriptomic research remains limited. Most previous studies on
386 human retinal aging have predominantly utilized conventional statistical approaches to identify
387 age-associated transcriptional changes[9,10,31]. Here, we generated scRNA-seq profiles from 18 unfrozen
388 retinas of a genetically homogeneous Chinese cohort spanning 34–92 years. By coupling conventional
389 differential-expression analysis with a cross-validated machine-learning framework, we delineate
390 conserved molecular hallmarks and expose sharp cell-type-specific vulnerabilities that refine the
391 molecular narrative of human retinal aging.

392 A key finding of our study was the progressive age-related reduction in the rod-to-cone ratio,
393 suggesting selective rod vulnerability. This aligns with classic histological and clinical observations
394 showing substantial rod loss by late adulthood [32,33]. Rods inherently possess higher metabolic demands
395 due to extensive outer segment renewal and their reliance on aerobic glycolysis, making them
396 particularly susceptible to metabolic stress, mitochondrial dysfunction, and oxidative damage [34,35]. Our
397 transcriptomic analysis provided direct molecular evidence supporting this hypothesis, demonstrating
398 substantial dysregulation of mitochondrial genes and oxidative phosphorylation pathways specifically
399 in rod. Quantitatively, rods exhibited significantly more mitochondrial-related DEGs compared to
400 cones. Additionally, marked inflammatory activation and upregulation of stress-response genes further
401 highlight rods' pronounced susceptibility to aging stressors [8]. In contrast, cones demonstrate fewer
402 transcriptional alterations, consistent with their known slower degenerative kinetics and greater
403 resilience [36,37]. Interestingly, cones selectively upregulated certain immune-related genes, possibly
404 reflecting adaptive responses rather than direct degeneration. Based on their relatively stable

transcriptomic profiles, cones may adopt distinct adaptive responses to mitigate the impact of aging-induced cellular stress.

Among retinal interneurons, BCs exhibited the most significant age-related transcriptional changes, prominently characterized by inflammatory activation and pronounced mitochondrial dysfunction. Animal studies have shown BC dendritic remodeling and altered synaptic ribbon architecture during aging [38], suggesting a heightened sensitivity of BCs to aging stress. HCs and ACs showed comparatively fewer transcriptional changes. Despite also exhibiting hallmarks of oxidative stress and synaptic remodeling, these interneurons may maintain greater intrinsic stability or resilience.

We also highlighted significant glial involvement in retinal aging, particularly MGCs, which displayed profound inflammatory responses and extracellular matrix remodeling. These findings support prior evidence that reactive gliosis in MGCs, initially protective, can exacerbate inflammation and vascular dysregulation upon chronic activation [39,40]. Astrocytes, although fewer in number, similarly exhibited stress-related activation. Enhanced astrocytic stress responses could reshape local inflammatory and metabolic environments, influencing neuronal survival and retinal homeostasis.

In contrast to traditional retinal aging studies that rely mainly on DE analysis to identify age-associated genes[41], ML approaches provide alternative methodologies that can extract informative signatures from noisy, high-dimensional data and alleviate certain statistical model assumptions[42]. While DE methods excel at detecting large-magnitude transcriptional changes, they frequently overlook subtle yet consistent alterations in regulatory elements and low-abundance transcripts that may be functionally significant. Traditional analyses rank genes by statistical significance, while machine learning provides feature importance rankings based on predictive power and biological relevance. Furthermore, while

general aging gene sets like SenMayo provide valuable insights into conserved senescence pathways [26], they may not fully capture the cell-type-specific nuances or the broader spectrum of non-senescence-related aging within a complex, specialized tissue such as the human retina. Our ML-ranking approach addresses this gap by identifying transcripts with the highest classification power, highlighting features that maintain consistent age-associated patterns even when their absolute expression changes fall below statistical thresholds for differential expression. This ML framework—from differential expression filtering to sparse modeling, recursive feature elimination, and stability validation—ensures both efficiency and reproducibility in identifying age-stage key genes for each cell type. By combining L1 regularization with RFECV, the framework struck a balance between model complexity and performance, while stability selection improves the biological relevance of the identified key genes. This complementary perspective helps bridge the gap between statistical significance and biological relevance in understanding retinal aging. These include metallothioneins, mitochondrial genes, proteostasis regulators, interferon-stimulated genes, chaperones, and long non-coding RNAs, many of which were not among the top DEGs but still emerged as robust indicators of aging. Importantly, the ML features also delineated cell type–resolved patterns: BCs, ACs, and rods shared a pronounced mitochondria-centric axis, whereas cones showed a retinoid metabolism, and proteostasis-focused profile. MGCs exhibited a coupled interferon-response and collagen signature, while HCs were marked by cytoskeletal and RNA-maintenance changes. By capturing these multifaceted and cell-specific signals beyond conventional DE analysis, the ML-driven approach provides a more precise, systems-level understanding of retinal aging and could inform more targeted therapeutic strategies.

This study has several limitations. The relatively small sample size in certain age brackets and the low RPE cell yield restrict our ability to capture RPE-specific aging changes. Proteomic and functional assays will be necessary to confirm these findings. Moreover, the ML models, while rigorously cross-validated, were trained on the same dataset used for feature discovery. For further study, independent external datasets will be essential to confirm the stability of the age-classifier gene sets.

In summary, we systematically characterized early-age transcriptional landscapes associated with human retinal aging within an ethnically homogeneous Chinese cohort. Our approach combined differential-expression statistics with a sparsity-driven machine-learning pipeline to identify robust aging signatures. This study addresses gaps previously overlooked in existing literature, particularly the focus on older starting ages and predominantly Caucasian representation. By generating the first machine-learning-derived, cell-type-specific aging gene lists for the human retina, our findings provide insights into conserved molecular hallmarks alongside distinctive cell-type-specific vulnerabilities relevant for developing targeted therapeutic interventions aimed at mitigating age-related retinal degeneration processes across diverse populations.

Statements and Declarations

Data availability

The single-cell RNA sequencing data generated in this study have been deposited in Figshare with the DOI: 10.6084/m9.figshare.28757048.

Author information

Authors and Affiliations

Nottingham Ningbo China Beacons of Excellence Research and Innovation Institute, University of Nottingham Ningbo China, Ningbo, China, 315100

Luning Yang, Sen Lin, Yiwen Tao, Qi Pan, Tengda Cai, Weihua Meng

Department of Ophthalmology, Lihuili Hospital affiliated with Ningbo University, Ningbo, China, 315040

Yunyan Ye

Department of Cardiology, Lihuili Hospital affiliated with Ningbo University, Ningbo, China, 315040

Jianhui Liu

Ningbo Institute of Innovation for Combined Medicine and Engineering, The Affiliated Li Huili Hospital, Ningbo University, Ningbo, China, 315201

Yang Zhou

Department of Ophthalmology, The Affiliated Ningbo Eye Hospital of Wenzhou Medical University, Ningbo, China, 315040

Quanyong Yi, Yongqing Shao

PAPRSB Institute of Health Sciences, Universiti Brunei Darussalam, Bandar Seri, Begawan, BE1410, Brunei Darussalam

Zen Huat Lu, Lie Chen

Centre for Public Health, Institute of Clinical Science, Queen's University Belfast, Block B, Royal Hospital, Grosvenor Road, Belfast, Northern Ireland, BT12 6BA

Gareth McKay

Centre for English Language Education, University of Nottingham Ningbo China, Ningbo, China, 315100

Richard Rankin

Eye Center, Zhongshan City People's Hospital, Zhongshan, Guangdong, China, 528403

Fan Li

Authors' Contributions

LY and SL drafted the paper and performed the analysis. YT, QP, TC contributed to data formatting and correction. YY, JL, YZ, YS, QY, ZL, LC, GM, and RR provided comments on the paper. FL, and WM organized the project and provided comments.

Acknowledgment

This study was mainly funded by the Pioneer and Leading Goose R&D Program of Zhejiang Province 2023 with reference number 2023C04049 and Ningbo International Collaboration Program 2023 with reference number 2023H025. Additionally, this work was supported by the National Natural Science Foundation of China with reference number 82201227 and the Natural Science Foundation of Guangdong Province, China with reference number 2023A1515011225.

Corresponding authors

Correspondence to Dr. Weihua Meng and Dr. Fan Li.

Consent to Publish

All authors have consent for publication.

Conflict of Interest

The authors have no conflicts of interest to disclose.

Ethics approval

This study was approved by the Ethics Committee of the University of Nottingham Ningbo China; The Lihuili Hospital affiliated with Ningbo University; The Affiliated Ningbo Eye Hospital of Wenzhou Medical University.

References

1. Marola, O.J., MacLean, M., Cossette, T.L., Diemler, C.A., Hewes, A.A., Reagan, A.M., Kanyinda, J.N., Skelly, D.A., and Howell, G.R. (2025). Genetic context modulates aging and degeneration in the murine retina. Molecular Neurodegeneration *20*, 8.
2. Popescu, I., Deelen, J., Illario, M., and Adams, J. (2023). Challenges in anti‐aging medicine–trends in biomarker discovery and therapeutic interventions for a healthy lifespan. Journal of cellular and molecular medicine *27*, 2643-2650.
3. Thapa, R., Khanal, S., Tan, H.S., Thapa, S.S., and van Rens, G.H.M.B. (2020). Prevalence, pattern and risk factors of retinal diseases among an elderly population in Nepal: the bhaktapur retina study. Clinical Ophthalmology, 2109-2118.
4. Di Carlo, E., and Augustin, A.J. (2021). Prevention of the onset of age-related macular degeneration. Journal of clinical medicine *10*, 3297.
5. Roberts-Martínez Aguirre, I., Rodríguez-Fernández, P., González-Santos, J., Aguirre-Juaristi, N., Alonso-Santander, N., Mielgo-Ayuso, J., and González-Bernal, J.J. (2022). Exploring the quality of life related to health and vision in a group of patients with diabetic retinopathy. In 1. (MDPI), pp. 142.
6. Abokyi, S., and Tse, D.Y.-y. (2025). Age-related driving mechanisms of retinal diseases and neuroprotection by transcription factor EB-targeted therapy. Neural regeneration research *20*, 366-377.
7. McLaughlin, T., Medina, A., Perkins, J., Yera, M., Wang, J.J., and Zhang, S.X. (2022). Cellular stress signaling and the unfolded protein response in retinal degeneration: mechanisms and therapeutic implications. Molecular Neurodegeneration *17*, 25.
8. Campello, L., Brooks, M.J., Fadl, B.R., Choi, H.S., Pal, S., and Swaroop, A. Transcriptional Heterogeneity and Differential Response of Rod Photoreceptor Pathway Uncovered by Single‐Cell RNA Sequencing of the Aging Mouse Retina. Aging Cell, e70001.
9. Yi, W., Lu, Y., Zhong, S., Zhang, M., Sun, L., Dong, H., Wang, M., Wei, M., Xie, H., and Qu, H. (2021). A single-cell transcriptome atlas of the aging human and macaque retina. National Science Review *8*, nwaa179.
10. Liu, H., Zhang, X., Wang, Q., Li, B., Bian, B., and Liu, Y. (2025). A Comprehensive Analysis of Sex-Biased Gene Expression in the Aging Human Retina Through a Combination of Single-Cell and Bulk RNA Sequencing. Investigative Ophthalmology & Visual Science *66*, 28-28.
11. Liang, Q., Cheng, X., Wang, J., Owen, L., Shakoor, A., Lillvis, J.L., Zhang, C., Farkas, M., Kim, I.K., and Li, Y. (2023). A multi-omics atlas of the human retina at single-cell resolution. Cell genomics *3*.
12. Wang, J., Cheng, X., Liang, Q., Owen, L.A., Lu, J., Zheng, Y., Wang, M., Chen, S., DeAngelis, M.M., and Li, Y. (2023). Single-cell multiomics of the human retina reveals hierarchical transcription factor collaboration in mediating cell type-specific effects of genetic variants on gene regulation. Genome biology *24*, 269.
13. Li, J., Wang, J., Ibarra, I.L., Cheng, X., Luecken, M.D., Lu, J., Monavarfeshani, A., Yan, W., Zheng, Y., and Zuo, Z. (2023). Integrated multi-omics single cell atlas of the human retina. Research Square, rs. 3. rs-3471275.
14. Bafiq, R., Mathew, R., Pearce, E., Abdel-Hey, A., Richardson, M., Bailey, T., and Sivaprasad, S. (2015). Age, sex, and ethnic variations in inner and outer retinal and choroidal thickness on

spectral-domain optical coherence tomography. American Journal of Ophthalmology *160*, 1034-1043. e1031.

15. Davey, P.G., Lievens, C., and Amonoo-Monney, S. (2020). Differences in macular pigment optical density across four ethnicities: a comparative study. Therapeutic advances in ophthalmology *12*, 2515841420924167.

16. Zouache, M.A., Silvestri, G., Amoaku, W.M., Silvestri, V., Hubbard, W.C., Pappas, C., Akafo, S., Lartey, S., Mastey, R.R., and Carroll, J. (2020). Comparison of the morphology of the foveal pit between African and Caucasian populations. Translational Vision Science & Technology *9*, 24-24.

17. McGinnis, C.S., Murrow, L.M., and Gartner, Z.J. (2019). DoubletFinder: doublet detection in single-cell RNA sequencing data using artificial nearest neighbors. Cell systems *8*, 329-337. e324.

18. Wolf, F.A., Angerer, P., and Theis, F.J. (2018). SCANPY: large-scale single-cell gene expression data analysis. Genome biology *19*, 1-5.

19. Gayoso, A., Lopez, R., Xing, G., Boyeau, P., Valiollah Pour Amiri, V., Hong, J., Wu, K., Jayasuriya, M., Mehlman, E., and Langevin, M. (2022). A Python library for probabilistic analysis of single-cell omics data. Nature biotechnology *40*, 163-166.

20. Butler, A., Hoffman, P., Smibert, P., Papalexi, E., and Satija, R. (2018). Integrating single-cell transcriptomic data across different conditions, technologies, and species. Nature biotechnology *36*, 411-420.

21. Love, M.I., Huber, W., and Anders, S. (2014). Moderated estimation of fold change and dispersion for RNA-seq data with DESeq2. Genome biology *15*, 1-21.

22. Fan, C., Chen, F., Chen, Y., Huang, L., Wang, M., Liu, Y., Wang, Y., Guo, H., Zheng, N., and Liu, Y. (2024). irGSEA: the integration of single-cell rank-based gene set enrichment analysis. Briefings in Bioinformatics *25*, bbae243.

23. Liberzon, A., Birger, C., Thorvaldsdóttir, H., Ghandi, M., Mesirov, J.P., and Tamayo, P. (2015). The molecular signatures database hallmark gene set collection. Cell systems *1*, 417-425.

24. Van de Sande, B., Flerin, C., Davie, K., De Waegeneer, M., Hulselmans, G., Aibar, S., Seurinck, R., Saelens, W., Cannoodt, R., and Rouchon, Q. (2020). A scalable SCENIC workflow for single-cell gene regulatory network analysis. Nature protocols *15*, 2247-2276.

25. Andreatta, M., and Carmona, S.J. (2021). UCell: Robust and scalable single-cell gene signature scoring. Computational and structural biotechnology journal *19*, 3796-3798.

26. Saul, D., Kosinsky, R.L., Atkinson, E.J., Doolittle, M.L., Zhang, X., LeBrasseur, N.K., Pignolo, R.J., Robbins, P.D., Niedernhofer, L.J., and Ikeno, Y. (2022). A new gene set identifies senescent cells and predicts senescence-associated pathways across tissues. Nature communications *13*, 4827.

27. Taghizadeh, E., Heydarheydari, S., Saberi, A., JafarpoorNesheli, S., and Rezaeijo, S.M. (2022). Breast cancer prediction with transcriptome profiling using feature selection and machine learning methods. BMC bioinformatics *23*, 410.

28. Saadh, M.J., Ahmed, H.H., Kareem, R.A., Yadav, A., Ganesan, S., Shankhyan, A., Sharma, G.C., Naidu, K.S., Rakhmatullaev, A., and Sameer, H.N. (2025). Advanced machine learning framework for enhancing breast cancer diagnostics through transcriptomic profiling. Discover Oncology *16*, 334.

29. Yuan, B., Yang, D., Rothberg, B.E., Chang, H., and Xu, T. (2020). Unsupervised and

supervised learning with neural network for human transcriptome analysis and cancer diagnosis. Scientific Reports *10*, 19106.

30. Krokidis, M.G., Vrahatis, A.G., Lazaros, K., Skolariki, K., Exarchos, T.P., and Vlamos, P. (2023). Machine learning analysis of Alzheimer's disease single-cell RNA-sequencing data across cortex and hippocampus regions. Current Issues in Molecular Biology *45*, 8652-8669.

31. Dhirachaikulpanich, D., Lagger, C., Chatsirisupachai, K., de Magalhães, J.P., and Paraoan, L. (2022). Intercellular communication analysis of the human retinal pigment epithelial and choroidal cells predicts pathways associated with aging, cellular senescence and age-related macular degeneration. Frontiers in Aging Neuroscience *14*, 1016293.

32. Curcio, C., Millican, C.L., Allen, K., and Kalina, R. (1993). Aging of the human photoreceptor mosaic: evidence for selective vulnerability of rods in central retina. Investigative ophthalmology & visual science *34*, 3278-3296.

33. Gao, H., and Hollyfield, J. (1992). Aging of the human retina. Differential loss of neurons and retinal pigment epithelial cells. Investigative ophthalmology & visual science *33*, 1-17.

34. Zhang, R., Shen, W., Du, J., and Gillies, M.C. (2020). Selective knockdown of hexokinase 2 in rods leads to age-related photoreceptor degeneration and retinal metabolic remodeling. Cell Death & Disease *11*, 885.

35. Jiang, K., Mondal, A.K., Adlakha, Y.K., Gumerson, J., Aponte, A., Gieser, L., Kim, J.-W., Boleda, A., Brooks, M.J., and Nellissery, J. (2022). Multiomics analyses reveal early metabolic imbalance and mitochondrial stress in neonatal photoreceptors leading to cell death in Pde6brd1/rd1 mouse model of retinal degeneration. Human molecular genetics *31*, 2137-2154.

36. Nag, T.C. (2021). Pathogenic mechanisms contributing to the vulnerability of aging human photoreceptor cells. Eye *35*, 2917-2929.

37. Scalabrino, M.L., Thapa, M., Chew, L.A., Zhang, E., Xu, J., Sampath, A.P., Chen, J., and Field, G.D. (2022). Robust cone-mediated signaling persists late into rod photoreceptor degeneration. Elife *11*, e80271.

38. Shrestha, A.P., Rameshkumar, N., Boff, J.M., Rajmanna, R., Chandrasegaran, T., Frederick, C.E., Zenisek, D., and Vaithianathan, T. (2023). The effects of aging on rod bipolar cell ribbon synapses. Cells *12*, 2385.

39. Kumar, A., Pandey, R.K., Miller, L.J., Singh, P.K., and Kanwar, M. (2013). Muller glia in retinal innate immunity: a perspective on their roles in endophthalmitis. Critical Reviews™ in Immunology *33*.

40. Balzamino, B.O., Cacciamani, A., Dinice, L., Cecere, M., Pesci, F.R., Ripandelli, G., and Micera, A. (2024). Retinal Inflammation and Reactive Müller Cells: Neurotrophins' Release and Neuroprotective Strategies. Biology *13*, 1030.

41. Soneson, C., and Robinson, M.D. (2018). Bias, robustness and scalability in single-cell differential expression analysis. Nature methods *15*, 255-261.

42. Brendel, M., Su, C., Bai, Z., Zhang, H., Elemento, O., and Wang, F. (2022). Application of deep learning on single-cell RNA sequencing data analysis: a review. Genomics, proteomics & bioinformatics *20*, 814-835.

647 **Figures**

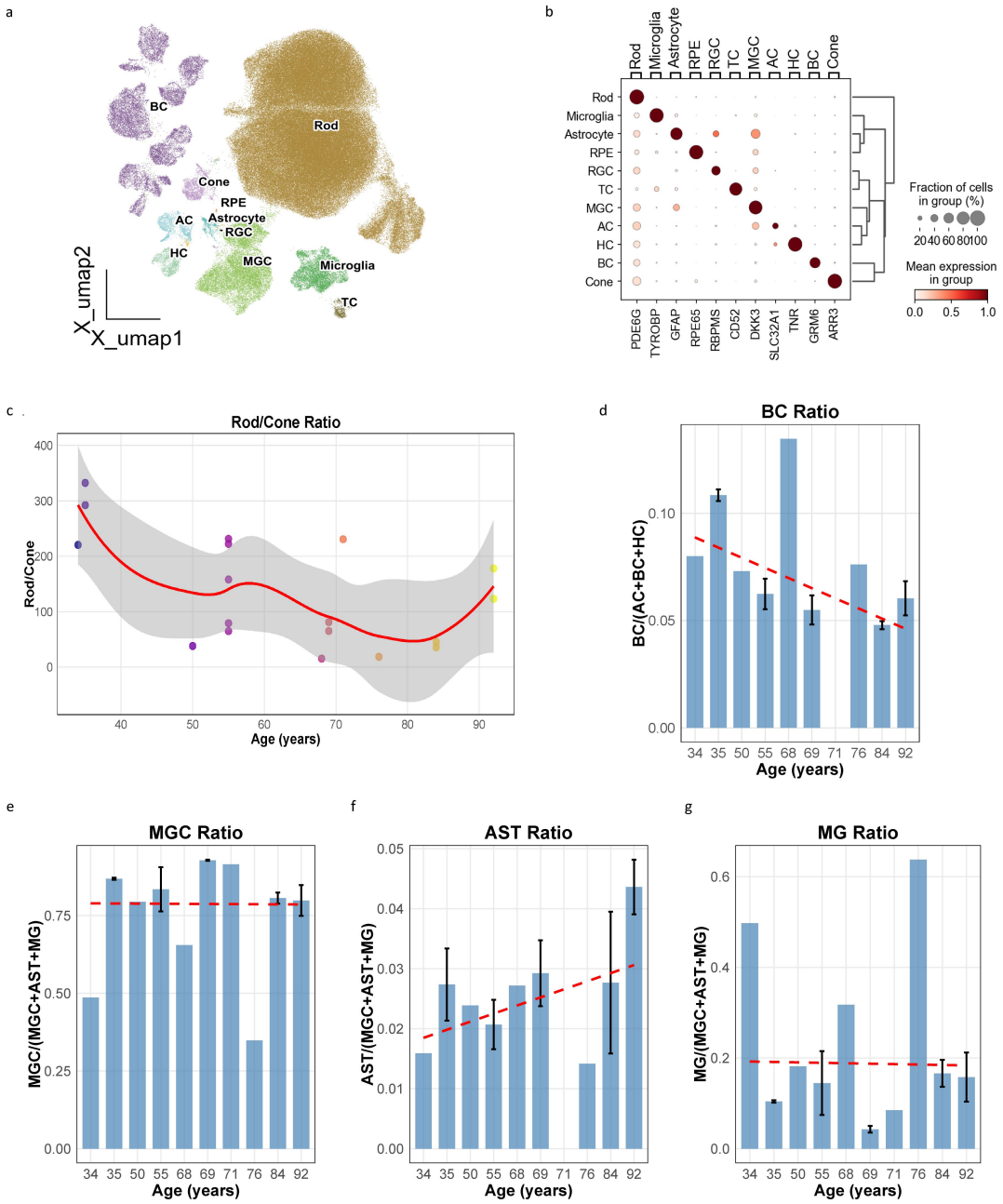

648

649 **Figure 1. (a)** UMAP visualization of 11 major retinal cell populations annotated from 18 samples. Cell

650 populations are color-coded by annotated cell types. **(b)** Dot plot showing marker genes' expression for

651 major retina cell type. Dot size represents the percentage of cells expressing each marker, while color

652 intensity indicates average expression level. **(c)** Scatter plot showing the age-dependent decline in

653 rod-to-cone photoreceptor ratio across individual samples. Each point represents an individual

654 sample. **(d)** Age-related changes in bipolar cell proportion relative to total interneurons (BC

655 /(AC+BC+HC)), showing a downward trend with advancing age. **(e)** Age-related changes in Müller

656 glial cells proportion relative to total glial cell populations (astrocytes, microglia, and Müller glial

657 cells). **(f)** Age-related changes in astrocytes proportion relative to total glial cell populations. **(g)**

658 Age-related changes in microglia proportion relative to total glial cell population.

659 AC: amacrine cell; BC: bipolar cell; HC: horizontal cell; MGC: Müller glial cell; RGC: retinal

660 ganglion cell; RPE: retinal pigment epithelium; TC: T cell; MG: Microglia; AST: Astrocyte

661

662

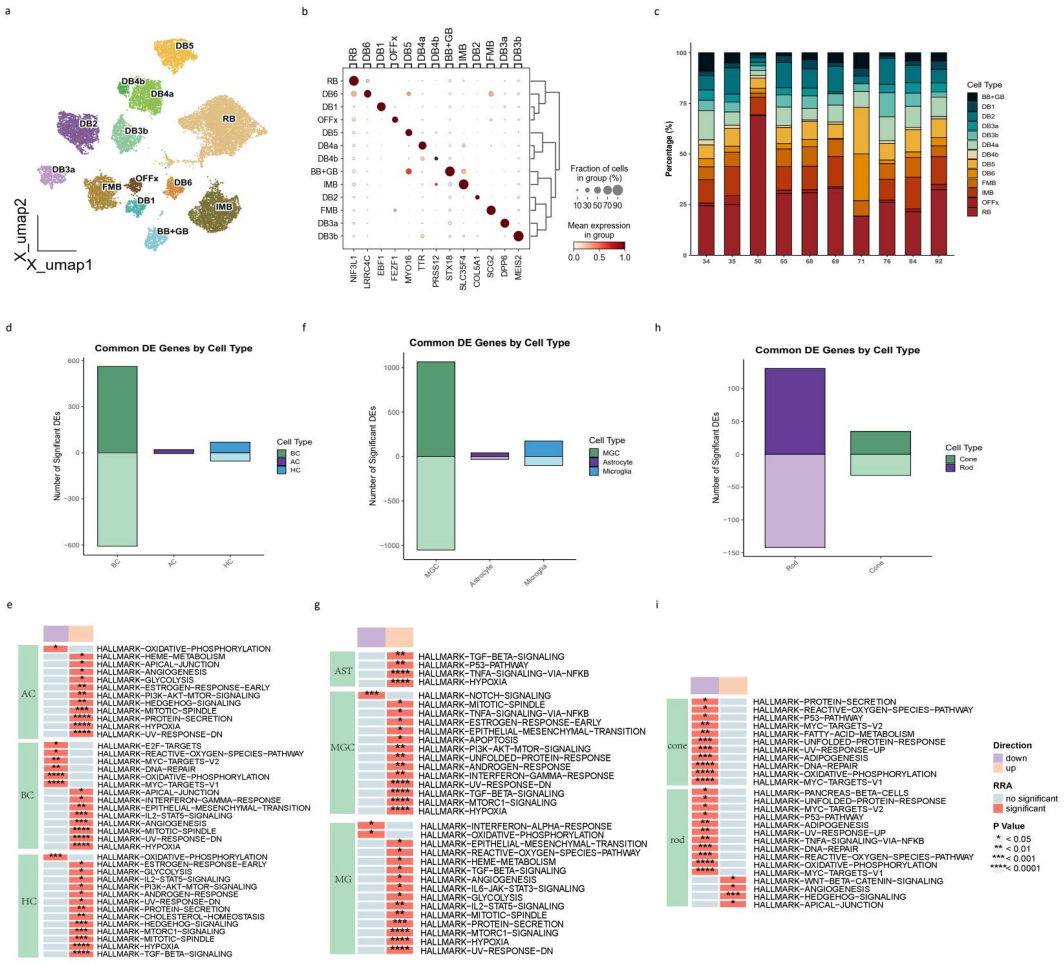

Figure 2. (a) UMAP visualization of bipolar cell subtypes. Distinct transcriptional clusters correspond to major bipolar cell subtypes, including rod bipolar cells (RB), ON diffuse bipolar cells (DB1−DB3a), OFF diffuse bipolar cells (DB3b−DB4), and midget bipolar cells—invaginating (IMB) and flat (FMB) types. **(b)** Dot plot showing marker genes' expression for bipolar cell subtypes. Dot size represents the percentage of cells expressing each marker gene, while color intensity indicates the average expression level. **(c)** Stacked bar chart depicting the relative proportions of bipolar cell subtypes across samples arranged by donor age. **(d, f, h)** Bar plot quantifying age-associated differentially expressed genes (DEGs) across retinal interneuron populations for (d) interneurons, (f) glia and (h) photoreceptors identified by integrated single-cell (SC-DE) and pseudobulk (PB-DE) analyses. Upward bars (positive

673 values) represent genes significantly upregulated in older retinas, while downward bars (negative
674 values) indicate genes significantly downregulated with age. **(e, g, i)** Heatmap showing enriched
675 pathways across retinal cell types of (e) interneurons, (g) glia and (i) photoreceptors based on irGSEA
676 analysis. Color intensity indicates robust rank aggregation score, with red representing upregulation
677 and blue representing downregulation. Significance levels: *P < 0.05, **P < 0.01, ***P < 0.001, ****P
678 < 0.0001.
679

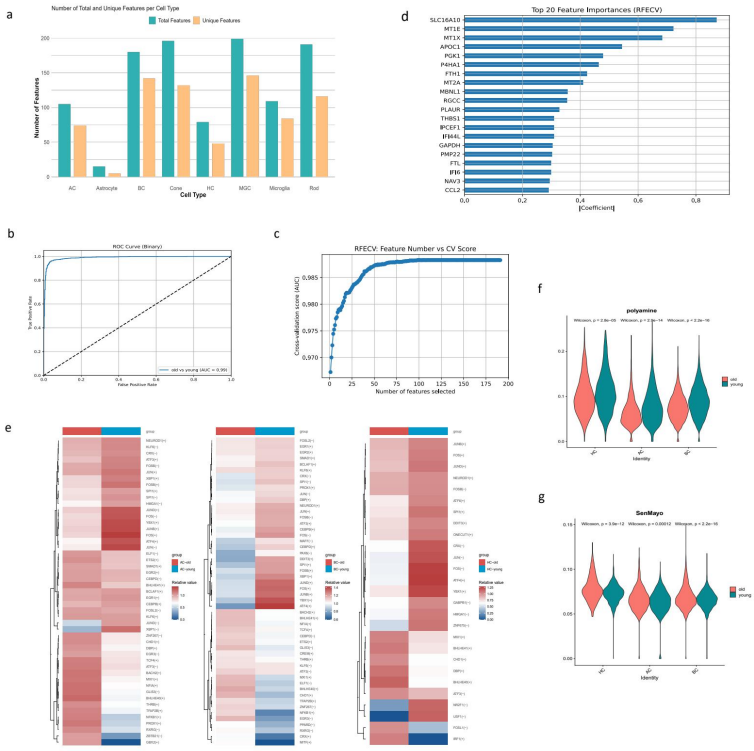

Figure 3. (a) Bar plot showing the number of machine learning-identified discriminatory features across different retinal cell types. Green bars represent the total number of ML features, while yellow bars represent cell-type-specific features unique to each cell type. **(b)** Receiver operating characteristic (ROC) curve demonstrating the performance of the machine learning classifier for distinguishing young versus old group of microglia, with area under the curve (AUC) indicating classification accuracy. **(c)** Recursive feature elimination with cross-validation (RFECV) plot showing the relationship between feature number and cross-validation accuracy scores for the aging classifier of microglia. **(d)** Horizontal bar chart displaying the top 20 feature importance scores for microglia age classification, ranked by their contribution to distinguishing young from old groups. Features represent genes with the highest discriminatory power for microglia aging. **(e)** Heatmap showing differential activity of transcription factor (TF) regulons between young and old groups across retinal interneuron types (amacrine cell, bipolar cell, and horizontal cell) identified by pySCENIC analysis. Each column represents an age group (old or young) within a specific cell type, while rows represent individual TF

694 regulons. Red indicates increased regulon activity in old retinas compared to young, while blue
695 indicates decreased activity. TFs are hierarchically clustered based on similarity in their activity
696 patterns across cell types. **(f)** Box plots comparing polyamine metabolism pathway scores between
697 young and old groups with P calculated by Wilcoxon rank-sum tests for each retinal glial interneuron.
698 **(g)** Box plots comparing cellular senescence gene set (SenMayo) activity scores between young and
699 old groups with P calculated by Wilcoxon rank-sum tests for each retinal interneuron.
700

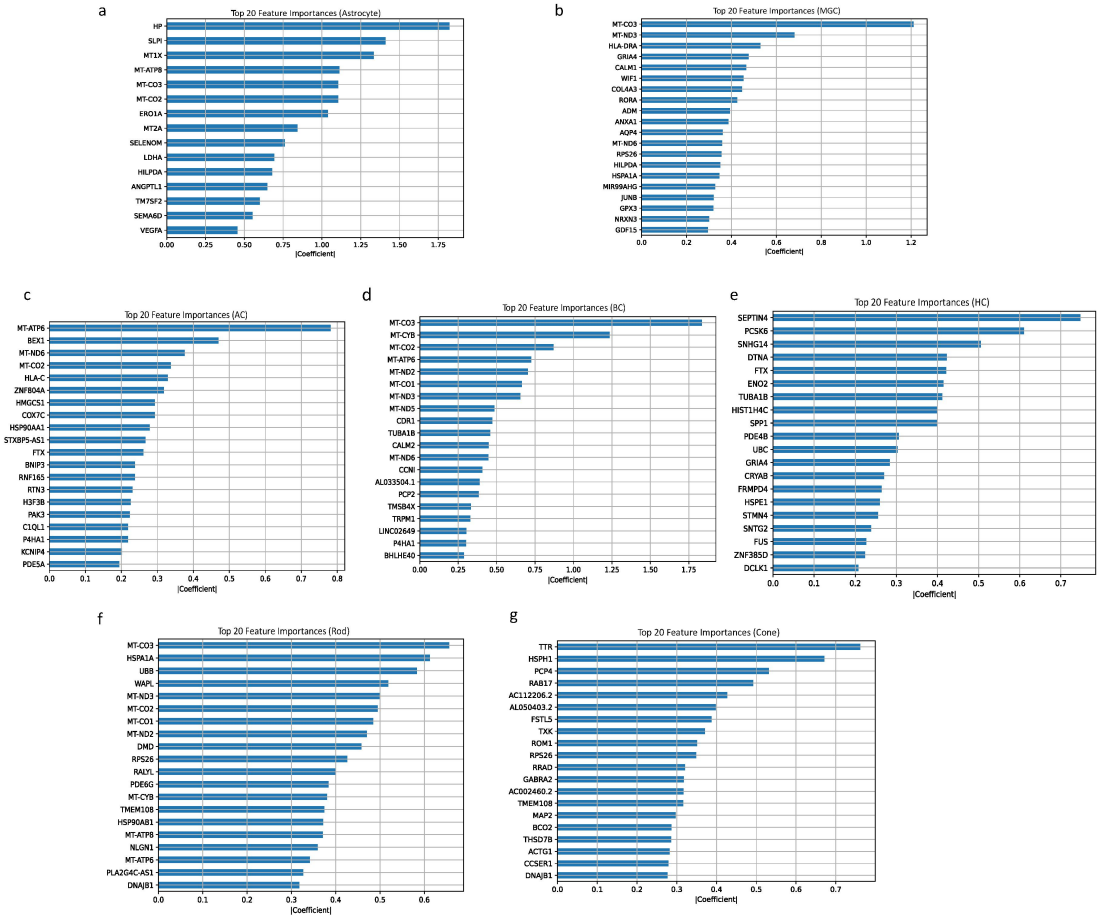

Figure 4. Horizontal bar charts showing the top 20 feature importance scores for age classification across different retinal cell types: (a) astrocytes, (b) Müller glial cells (MGCs), (c) amacrine cells (ACs), (d) bipolar cells (BCs), (e) horizontal cells (HCs), (f) rod photoreceptors, and (g) cone photoreceptors.

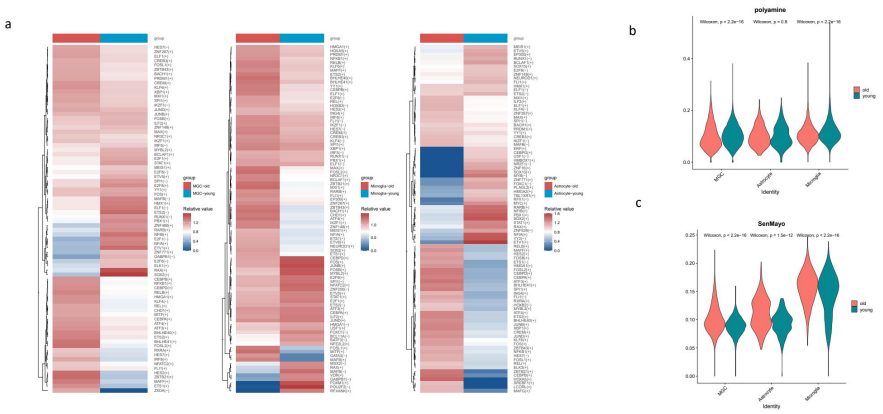

Figure 5. (a) Heatmap showing differential activity of transcription factor (TF) regulons between young and old groups across retinal glial celltypes (astrocyte, Müller glial cells and microglia) identified by pySCENIC analysis. Each column represents an age group (old or young) within a specific cell type, while rows represent individual TF regulons. Red indicates increased regulon activity in old retinas compared to young, while blue indicates decreased activity. TFs are hierarchically clustered based on similarity in their activity patterns across cell types. **(b)** Box plots comparing polyamine metabolism pathway scores between young and old groups with P calculated by Wilcoxon rank-sum tests for each retinal glial cell type. **(c)** Box plots comparing cellular senescence gene set (SenMayo) activity scores between young and old groups with P calculated by Wilcoxon rank-sum tests for each retinal glial cell type.

Table S1: Gene sets used for scoring analyses.

Table S2: Composition of major retinal cell types across the 18 samples.

Table S3: Composition of bipolar cell subtypes across the 18 samples.

Table S4: Differentially expressed genes identified through both single-cell differential expression and pseudobulk differential expression analyses across 3 retinal interneuron populations: amacrine cells, horizontal cells, and bipolar cells.

Table S5: Differentially expressed genes identified through both single-cell differential expression and pseudobulk differential expression analyses across 3 retinal glial populations: Müller glial cells, astrocytes, and microglia.

Table S6: Differentially expressed genes identified through both single-cell differential expression and pseudobulk differential expression analyses across 2 retinal photoreceptor populations: rods, and cones.

Table S7: List of ML selected aging features for each cell type, ranked by importance.

Table S8: List of ML selected aging features recurring in more than two cell types with frequency counts.

Table S9: Transcription factor regulon activity across retinal interneuron populations during aging.

Table S10: Transcription factor regulon activity across retinal glial populations during aging.

Table S11: Transcription factor regulon activity across retinal photoreceptor populations during aging.

738 **Table 1.** Retinal sample information

Sample	Tissue Source	Eye‡	Sex§	Age(y)	Diabetic Status*	Eye Removal/Death Reason	Hospital†	Group
1	Live	L	M	76	DM	Corneal staphyloma	L.H.	Old
2	Live	L	M	55	nonDM	Phthisis bulbi	L.H.	Young
3	Live	R	M	71	nonDM	Corneal ulcer	Y.H.	Old
4	Live	L	F	50	nonDM	Phthisis bulbi	Y.H.	Young
5	Live	R	F	68	nonDM	Corneal perforation	Y.H.	Old
6	Cadaver	L	M	34	nonDM	Cerebral hemorrhage	Y.H.	Young
7	Cadaver	L	F	92	nonDM	Natural death	Y.H.	Old
8	Cadaver	R	F	92	nonDM	Natural death	Y.H.	Old
9	Cadaver	L	F	55	DM	Traumatic brain injury	Y.H.	Young
10	Cadaver	R	F	55	DM	Traumatic brain injury	Y.H.	Young
11	Cadaver	L	M	55	DR	Brainstem hemorrhage	Y.H.	Young
12	Cadaver	R	M	55	DR	Brainstem hemorrhage	Y.H.	Young
13	Cadaver	L	M	35	DR	Traumatic shock	Y.H.	Young
14	Cadaver	R	M	35	DR	Traumatic shock	Y.H.	Young
15	Cadaver	L	M	84	DR	Prostate cancer	Y.H.	Old
16	Cadaver	R	M	84	DR	Prostate cancer	Y.H.	Old
17	Cadaver	L	M	69	DR	Lung cancer	Y.H.	Old
18	Cadaver	R	M	69	DR	Lung cancer	Y.H.	Old

739 *DM, diabetes mellitus without diabetic retinopathy DR; diabetic retinopathy; nonDM, non-diabetic retinopathy nor diabetic. Because the tissues were obtained
740 intra-operatively or post-mortem and detailed fundus imaging records were unavailable, the exact stage or subtype of diabetic retinopathy (e.g., NPDR vs PDR) could not be
741 ascertained for the DR cases.
742 †L.H., The Ningbo Lihuili Hospital; Y.H., The Ningbo Eye Hospital.
743 ‡ L, left; R, right.

§M, male; F, female.

Table 2. Performance Metrics of Cell Age Classification Models Across Retinal Cell Types

Cell Type‡	Accuracy*	F1-Score†	Precision†	Recall†	AUC
Microglia	0.96	0.95	0.95	0.95	0.98
HC	0.93	0.93	0.93	0.93	0.97
BC	0.91	0.91	0.91	0.90	0.96
Cone	0.90	0.88	0.89	0.87	0.94
Rod	0.89	0.89	0.89	0.89	0.95
MGC	0.89	0.89	0.89	0.89	0.95
AC	0.85	0.83	0.84	0.82	0.93
Astrocyte	0.80	0.79	0.79	0.79	0.87

*Accuracy represents the overall proportion of correctly classified cells.

†F1-score, precision, and recall are reported as macro-averages across young and old classes.

‡ HC: horizontal cell; BC: bipolar cell; MGC: Müller glial cell; AC: amacrine cell.